

Synthesis, adsorption, thermodynamic studies and corrosion inhibition behaviour of isoniazide derivatives on mild steel in hydrochloric acid solution

M. P. Chakravarthy¹, K. N. Mohana^{1*} and C. B. Pradeep Kumar²

¹(Department of Studies in Chemistry, University of Mysore, Manasagangothri, Mysore-570 006, India)

²(Post Graduate Department of Chemistry, Sarada Vilas College, Mysore-570 005, India)

Abstract: Corrosion inhibition behaviour of a new class of isoniazide derivatives on mild steel in 0.5 M HCl was evaluated by electrochemical and non-electrochemical techniques. The Langmuir adsorption isotherm model was taken into account since equilibrium adsorption of all the three corrosion inhibitors was found to obey this adsorption isotherm model. The difference in modes of adsorption and inhibition efficiency of these inhibitors depend on the chemical composition, molecular structure, nature of the metal surface and electrochemical potential values of metal-solution interface. Potentiodynamic polarization studies clearly revealed that all the three inhibitors are of mixed type. Various thermodynamic parameters for the adsorption of these inhibitors on mild steel were computed and discussed. Electrochemical measurements and mass loss measurements are in good agreement with each other. The equilibrium adsorption mechanisms and morphological studies of inhibited and uninhibited metal surfaces were examined by FTIR, EDX and SEM analyses.

Keywords: Adsorption, Corrosion, Electrochemical impedance spectroscopy, Isoniazide derivatives, Mild steel, Potentiodynamic polarization

I. Introduction

The investigation of corrosion of mild steel (MS) is a subject of high theoretical as well as practical interest. Mild steel and its alloys are widely used as engineering materials because of its low cost and good mechanical properties. However, it is highly susceptible to corrosion especially in acid media^[1]. Mineral acids are commonly used in industries for pickling, acid cleaning, acid de-scaling of boilers, heat exchangers, cooling towers, etc., to remove scales, deposits and other corrosion products^[2]. Corrosion problem occurs in these industries and can cause disastrous damage to metal and alloy structures causing economic consequences in terms of repair, replacement and product losses. Inhibitors are commonly used to reduce the corrosive attack on metallic materials in acidic and neutral conditions^[3, 4].

A wide variety of organic compounds have been extensively used as corrosion inhibitors. The inhibition properties of these compounds are attributed to their molecular structures, planarity and the lone pairs of electrons present on the hetero atoms, which determine the adsorption of these molecules on the metallic surfaces. The presence of corrosion inhibitors in small amount brings morphological changes in the metal surface by reducing the corrosion rate. Corrosion inhibitors block the active sites and enhance the adsorption process, thus decreasing the corrosion rate and extending the life span of the equipment^[5, 6]. It was observed that the efficiency of an inhibitor not only depends on its structure, but also on the characteristics of the environment in which it is considered and the experimental conditions. The most efficient inhibitors are organic compounds containing electronegative functional groups and π -electrons in triple or conjugated double bonds having a tendency to resist corrosion^[7, 8]. Compounds rich in hetero atoms can be regarded as environmental friendly corrosion inhibitors because of their strong chemical activity and low toxicity^[9]. The adsorption characteristics of organic molecules are also affected by sizes, electron density at the donor atoms and orbital character of donating electrons^[10-12]. Compounds containing both nitrogen and sulphur atoms are of particular importance as they often provide excellent inhibition compared with compounds containing only nitrogen or sulphur by bringing down the hydrogen permeation current to a considerable extent.

The organic compounds containing hetero atoms and multiple bonds such as 1,3,4-oxadiazole derivatives^[13], poly(ethylene terephthalate)^[14], fatty acid oxadiazole derivatives^[15], sulphonamide compounds^[16], thiadiazoles derivatives^[17], fluoroquinolones^[18], aminopyridine derivatives^[19], fatty acid triazole derivatives^[20] and lauric hydrazide derivatives^[21] have been reported as effective corrosion inhibitors in acidic condition.

The present study was undertaken to investigate the influence of the three newly synthesized isoniazide derivatives such as N²-(thiophen-2-ylmethylene)isonicotinohydrazide (INTMH), N¹-isonicotinoyl-N-methyl-N-phenylformohydrazonamide (INMFA) and N-isonicotinoylbenzohydrazonothioic acid (INBHT) on the

dissolution of MS in 0.5 M HCl using mass loss and electrochemical methods. The effect of temperature on the dissolution of MS in uninhibited and inhibited acid solutions was investigated. Various activation and adsorption thermodynamic parameters were computed and discussed. The passive film formed on the MS surface was characterized by FTIR, EDX and SEM techniques. Further, the inhibition performance of the three derivatives have been compared and discussed.

II. Experimental

2.1 Mild steel specimen preparation

MS specimens used in the present study has the following chemical compositions (in weight %): 0.051% C, 0.179% Mn, 0.006% Si, 0.051% Cr, 0.05% Ni, 0.013% Mo, 0.004% Ti, 0.103% Al, 0.050% Cu, 0.004% Sn, 0.00105% B, 0.017% Co, 0.012% Nb, 0.001% Pb and the remainder iron. For all experiments, square type MS specimens of dimension 2 cm × 2 cm × 0.1 cm were used. The specimens were mechanically well polished with different grades SiC (200 - 600) emery papers, degreased with benzene, washed with triply distilled water and finally dried. All the solvents and chemicals used were of AR grade, and used as such. Triply distilled water was used in the preparation of the various concentrations of test solutions.

2.2 Synthesis of inhibitors

INTMH was synthesized by dissolving 0.68 g (5 mmol) isoniazide (C₆H₇N₃O, Mol. Wt. 137.34) in 15 mL of ethanol in a round bottom flask. To this 0.46 mL (5 mmol) of 2-thiophene-carboxaldehyde (C₅H₄OS, Mol. Wt. 112.15) in 15 mL ethanol was mixed and refluxed for 6 hr at room temperature in the presence of glacial acetic acid and then the solution was concentrated using rotor vaporizer and kept for drying in vacuum. INMFA was synthesized by dissolving 0.68 g (5 mmol) of isoniazide in 15 mL of ethanol in a round bottom flask. To this a 0.62 mL (5 mmol) of N-methylformanilide (C₈H₉NO, Mol. Wt. 135.16) dissolved in 15 mL of ethanol was added and refluxed for 6 hrs with stirring at room temperature in the presence of glacial acetic acid. Then the solution was concentrated using rotor vaporizer and kept for drying in vacuum and the product obtained was collected.

INBHT was synthesized by dissolving 0.68 g (5 mmol) of isoniazide in 15 mL of ethanol in a round bottom flask. To this 0.59 mL (5 mmol) of thiobenzoic acid (C₇H₆OS, Mol. Wt. 138.18) in 15 mL ethanol was mixed and refluxed for 6 hr at room temperature in the presence of glacial acetic acid, and then the solution was concentrated using rotor vaporizer and kept for drying in vacuum. The synthetic scheme of INTMH, INMFA and INBHT are shown in fig. (1)

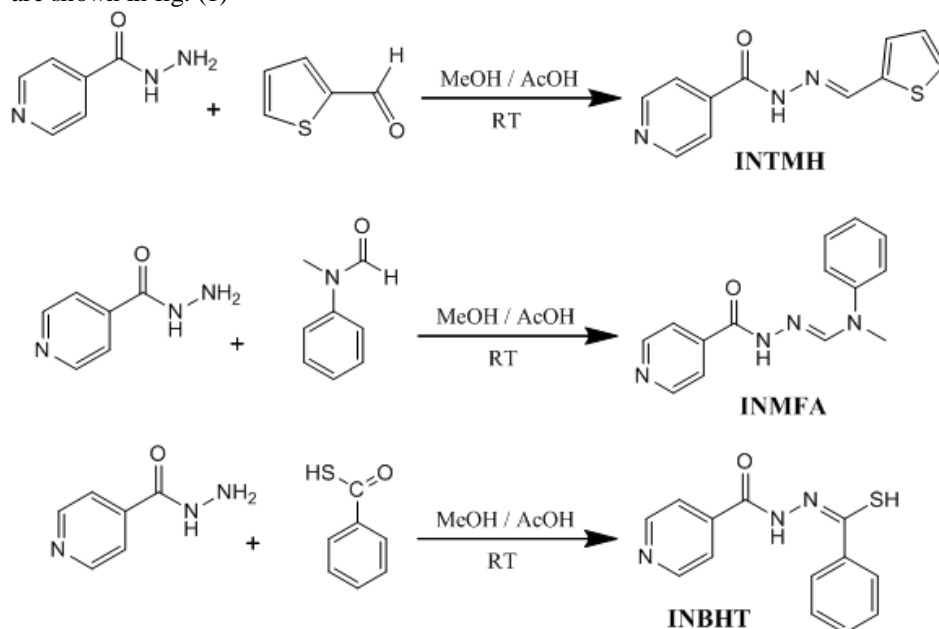


Figure (1): Synthetic schemes of INTMH, INMFA and INBHT.

All the synthesized compounds were characterized by FTIR, ¹H-NMR and Mass spectral studies. INTMH (C₁₁H₉N₃OS, Mol. Wt. 231.27): Yield: 93%, Melting Range (M. R, °C): 186-190. FTIR (KBr, cm⁻¹): 720 (C-S), 1662 (N=C), 1761 (C=O). ¹H-NMR (400.15 MHz, DMSO-d₆) δ ppm: δ 7.17 (t, J = 4.60 Hz, 1H), 7.53 (d, J = 3.52 Hz, 1H), 7.72 (d, J = 5.04 Hz, 1H), 7.81 (dd, J = 1.60, 4.44 Hz, 2H), 8.68 (s, 1H), 8.79 (dd, J = 1.56, 4.46 Hz, 2H), 12.03 (s, 1H). MS, m/z: 232 (M+1). Elemental analyses found (calculated) for C₁₁H₉N₃OS (%): C, 57.09 (57.13); H, 3.87 (3.92); N, 18.09 (18.17), O, 6.85 (6.92), S, 13.78 (13.86).

INMFA (C₁₄H₁₄N₄O, Mol. Wt. 254.29): Yield: 89%, Melting Range (M. R, °C): 138-140. FTIR (KBr, cm⁻¹): 1628 (N=C), 1750 (C=O). ¹H-NMR (400.15 MHz, DMSO-d₆) δ ppm: δ 2.82 (s, 3H), 6.42-6.47 (m, 2H), 7.12-7.16 (m, 3H), 7.79 (dd, J = 1.68, 4.77 Hz, 2H), 8.42 (s, 1H), 8.98 (dd, J = 1.64, 4.58 Hz, 2H), 12.05 (s, 1H). MS, m/z: 255 (M+1). Elemental analyses found (calculated) for C₁₄H₁₂N₂OS (%): C, 66.05 (66.13); H, 5.49 (5.55); N, 21.99 (22.03), O, 6.22 (6.29).

INBHT (C₁₃H₁₁N₃OS, Mol. Wt. 257.31): Yield: 90%, Melting Range (M. R, °C): 230-232. FTIR (KBr, cm⁻¹): 707 (C-S), 1640 (N=C), 1692 (C=O). ¹H-NMR (400.15 MHz, DMSO-d₆) δ ppm: δ 1.52 (s, 1H), 6.92-6.97 (m, 3H), 7.32-7.37 (m, 2H), 7.80 (dd, J = 1.58, 4.67 Hz, 2H), 8.97 (dd, J = 1.54, 4.54 Hz, 2H), 11.85 (s, 1H). MS, m/z: 258 (M+1). Elemental analyses found (calculated) for C₁₃H₁₀N₂OS (%): C, 60.61 (60.68); H, 4.27 (4.31); N, 16.27 (16.33), O, 6.16 (6.22), S, 12.41 (12.46). Melting range was determined by Veego Melting Point VMP III apparatus. FTIR spectra were recorded using a Jasco FTIR 4100 double beam spectrophotometer. ¹H-NMR spectra were recorded on Bruker DRX-500 spectrometer at 400 MHz using DMSO-d₆ as solvent and TMS as an internal standard. Mass spectral data were obtained by LC/MSD Trap XCT. Elemental analyses were recorded on Vario-MICRO superuser V1.3.2 Elementar.

2.3 Mass loss measurements

Mass loss measurements were performed by weighing the cleaned and dried MS specimens before and after immersion in 0.5 M HCl solutions from one to five hours in the absence and presence of various concentrations of INTMH, INMFA and INBHT at different temperatures (30 – 60 °C). Triplicate experiments were performed in each case and the mean value of the mass loss was noted. Corrosion rate (CR) in mg cm⁻² h⁻¹ and inhibition efficiency η (%) were calculated using the following equations:

$$CR = \frac{\Delta W}{S \tau} \quad (1)$$

where ΔW is the weight loss, S is the surface area of the specimen and t is immersion time.

$$\eta (\%) = \frac{(CR)_a - (CR)_p}{(CR)_a} \times 100 \quad (2)$$

where (CR)_a and (CR)_p are the corrosion rates in the absence and the presence of the inhibitor, respectively.

2.4 Potentiodynamic polarization measurements

Potentiodynamic polarization measurements were carried out with well polished and cleaned MS specimen as working electrode in 0.5 M HCl solutions with different inhibitor's concentrations (200 – 500 ppm) with an exposed area of 1 cm² and this working area was remained precisely fixed throughout the experiment. A conventional three electrode cell consisting of MS as working electrode, platinum foil as counter electrode and saturated calomel electrode (SCE) as reference electrode was used. All potentials were measured against SCE. Potentiodynamic polarization studies were carried out using CH-instrument (model CHI660D). Before each Tafel experiment, the MS electrode was allowed to corrode freely and its open circuit potential (OCP) was recorded as a function of time up to 30 min. After this time, a steady state OCP corresponding to the corrosion potential (E_{corr}) of the working electrode was obtained. The polarization curves were recorded by changing the electrode potential automatically at a scan rate of 0.2 mV/s. The η (%) was calculated from corrosion currents determined from the Tafel extrapolation plot method using the experimental relation (3).

$$\eta(\%) = \frac{(I_{corr})_a - (I_{corr})_p}{(I_{corr})_a} \times 100 \quad (3)$$

where (I_{corr})_a and (I_{corr})_p are the corrosion current density (μA cm⁻²) in the absence and the presence of the inhibitor, respectively.

2.5 Electrochemical impedance spectroscopy (EIS)

Electrochemical impedance measurements were carried out using the same CH-instrument. The EIS data were taken in the frequency range 10 kHz to 100 mHz. The double layer capacitance (C_{dl}) and the polarization resistance (R_p) were determined from Nyquist plots. The percentage inhibition efficiency, η (%) was calculated from R_p values using the following expression:

$$\eta(\%) = \frac{1/(R_p)_a - 1/(R_p)_p}{1/(R_p)_a} \times 100 \quad (4)$$

where (R_p)_a and (R_p)_p are polarization resistances in the absence and the presence of the inhibitor, respectively.

2.6 FTIR, EDX and SEM studies

The surface analyses of uninhibited and inhibited MS specimens were carried out using FTIR, EDX and SEM studies. The MS specimens were immersed in 0.5 M HCl in the presence of inhibitors (500 ppm) for a period of 1 hr. Then the specimens were taken out and dried. The surface adhered film was scrapped carefully

and its IR spectra were recorded using a Jasco FTIR 4100 double beam spectrophotometer. The surface feature of the MS specimens in the absence and the presence of inhibitors were studied by energy dispersive X-ray spectroscopy (EDX) and scanning electron microscope (model JSM-5800).

III. Results and Discussion

3.1 Mass loss studies

The CR and η (%) in the absence and presence of various concentrations of INTMH, INMFA and INBHT in 0.5 M HCl solution at different temperatures (30 – 60 °C) are presented in Table (1). Inspection of mass loss data revealed the linear variation of weight loss with temperature, concentration and time in inhibited and uninhibited 0.5 M HCl. The mass loss was found to be decreased and η (%) increased with increase in concentration of isoniazide derivatives. The maximum inhibition efficiency was found at 500 ppm.

Table (1): CR and η (%) obtained from mass loss measurements of MS in 0.5 M HCl solution containing various concentrations of INTMH, INMFA and INBHT at different temperatures

T (°C)	C (ppm)	INTMH		INMFA		INBHT	
		CR (mg cm ⁻² h ⁻¹)	η (%)	CR (mg cm ⁻² h ⁻¹)	η (%)	CR (mg cm ⁻² h ⁻¹)	η (%)
30	Blank	0.7200	-	0.7200	-	0.7200	-
	200	0.1605	77.74	0.1409	80.45	0.1193	83.45
	300	0.1165	83.84	0.0916	87.29	0.0699	90.29
	400	0.1003	86.08	0.0790	89.04	0.0572	92.05
	500	0.0707	90.19	0.0533	92.60	0.0317	95.60
40	Blank	0.9490	-	0.9490	-	0.9490	-
	200	0.2257	76.20	0.1991	79.00	0.1708	81.99
	300	0.1816	80.84	0.1585	83.28	0.1300	86.28
	400	0.1484	84.35	0.1181	87.54	0.0897	90.53
	500	0.1134	88.04	0.0860	90.93	0.0576	93.92
50	Blank	1.1520	-	1.1520	-	1.1520	-
	200	0.2953	74.36	0.2597	77.45	0.2251	80.45
	300	0.2461	78.63	0.2070	82.02	0.1725	85.021
	400	0.2119	81.60	0.1647	85.69	0.1302	88.68
	500	0.1539	86.63	0.1183	89.72	0.0839	92.71
60	Blank	1.4350	-	1.4350	-	1.4350	-
	200	0.3998	72.14	0.3585	75.02	0.3155	78.02
	300	0.3173	77.89	0.2672	81.37	0.2242	84.37
	400	0.2843	80.19	0.2394	83.31	0.1958	86.35
	500	0.2220	84.53	0.1728	87.96	0.1296	90.97

Further increase in concentration (beyond 500 ppm) did not cause any remarkable change in the inhibition efficiency. There is no appreciable increase in the inhibition efficiency after 1hr of immersion time, this is due to desorption of the inhibitor molecules from the metal surface with increasing immersion time and instability of the inhibitor film on the metal surface [22, 23]. The formation of protective film by inhibitor adsorption on the MS surface is reinforced with immersion time and is relatively fast and completed in 1 hr. The inhibition efficiency was found to depend on the concentration of the inhibitor and nature of the substituent in the molecule. In all the studied inhibitors, the increase in the concentration was accompanied by a decrease in weight loss and increase in the percentage inhibition efficiency.

3.2 Effect of temperature

The effect of temperature on CR and η (%) was studied in the temperature range of 30 – 60 °C in the absence and the presence of different concentrations of inhibitors (table 1). The results show that the corrosion rates in both inhibited and uninhibited solutions increased with rise in temperature from 30 – 60 °C. This indicates that the inhibition occurs through the adsorption of the inhibitors on the metal surface and description is aided by increasing temperature. The activation parameters for the corrosion process are calculated from the Arrhenius type plot according to the following equation:

$$CR = k \exp^{-E_a/RT} \tag{5}$$

where E_a is the apparent activation energy for corrosion process, k is the Arrhenius pre-exponential factor, T is the absolute temperature and R is the universal gas constant. The values of E_a without and with various concentrations of inhibitors are obtained from the slope of the plot of log CR versus 1/T (fig. 2) and are shown in Table (2). E_a values for inhibited systems are higher than those for the uninhibited system suggest that dissolution of MS is slow [24].

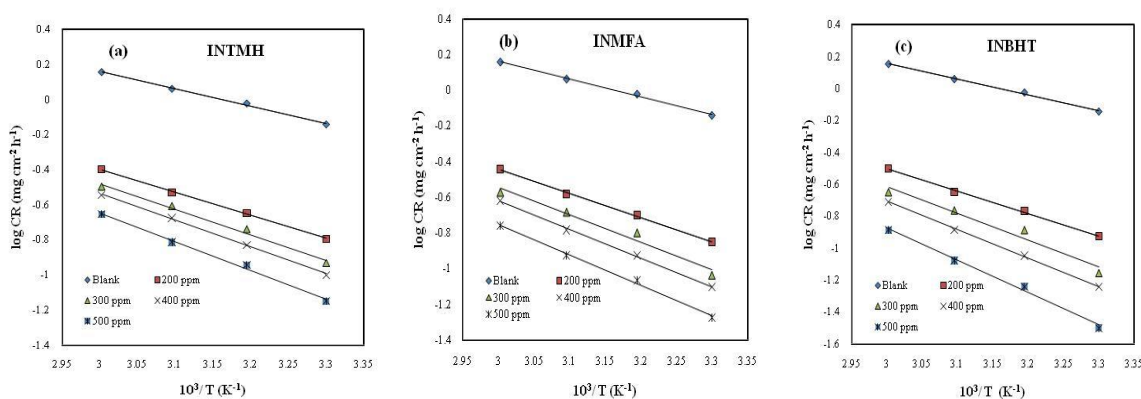


Figure (2): Plot of log CR versus 1/T for (a) INTMH (b) INMFA and (c) INBHT.

Table (2): Values of activation parameters for MS in 0.5 M HCl medium in the absence and presence of various concentrations INTMH, INMFA and INBHT

Inhibitor	C (ppm)	E _a (kJ mol ⁻¹)	ΔH _a (kJ mol ⁻¹)	ΔH _a = E _a - RT (kJ mol ⁻¹)	ΔS _a (J mol ⁻¹ K ⁻¹)
Blank	0	19.00	16.36	16.48	-197.57
INTMH	200	25.21	22.57	22.69	-185.72
	300	27.83	25.19	25.32	-179.42
	400	29.21	26.57	26.69	-176.35
	500	31.38	28.75	28.86	-171.99
INMFA	200	25.71	23.07	23.19	-185.16
	300	29.31	26.67	26.79	-176.30
	400	30.69	28.05	28.17	-173.58
	500	32.28	29.63	29.76	-171.41
INBHT	200	26.76	24.12	24.24	-183.09
	300	31.84	29.21	29.32	-170.02
	400	34.06	31.42	31.54	-165.12
	500	38.63	36.01	36.11	-154.58

It was found that, as the concentration of the inhibitor increases, the values of E_a also increases. This means the presence of inhibitor induces an energy barrier for corrosion reaction and this barrier increases with increasing concentration of the inhibitors.

Alternative Arrhenius plots of log CR/T versus 1/T (fig. 3) for MS dissolution in 0.5 M HCl in the absence and presence of different concentrations of INTMH, INMFA and INBHT were used to calculate the values of activation thermodynamic parameters such as enthalpy of activation (ΔH_a) and entropy of activation (ΔS_a) using the relation (6),

$$CR = \frac{RT}{Nh} \exp\left(\frac{\Delta S_a}{R}\right) \exp\left(\frac{-\Delta H_a}{RT}\right) \quad (6)$$

where R is the universal gas constant, T is the absolute temperature, N is the Avogadro's number, h is Planks constant. The values of ΔH_a and ΔS_a were obtained from the slope and intercept of the above plot, and presented in table (2). The obtained ΔH_a values are in good agreement with those calculated from the equation (7).

$$\Delta H_a = E_a - RT \quad (7)$$

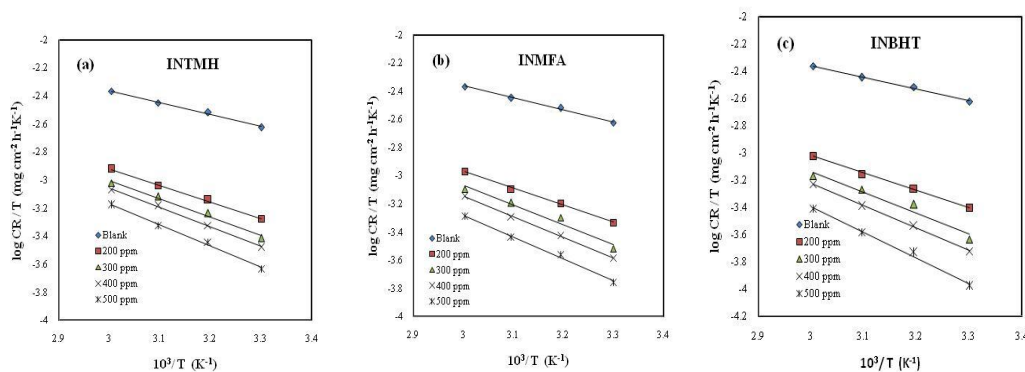


Figure (3): Alternative Arrhenius plots for MS dissolution in 0.5 M HCl medium in the absence and presence of (a) INTMH (b) INMFA and (c) INBHT.

The positive shift of enthalpy of activation (ΔH_a) reflects that the process of adsorption of inhibitors on MS surface is endothermic process. The values of entropy of activation (ΔS_a) are higher for inhibited solutions than that for the uninhibited solution reflecting an increase in randomness on going from reactants to the activated complex. The increase in ΔS_a values by the adsorption of inhibitor molecules on the MS surface in acid solution could be regarded as quasi-substitution between the inhibitors in the aqueous phase and water molecules on the metal surface. In such condition, the adsorptions of inhibitor molecules follow desorption of water molecules from the metal surface and hence decrease the electrical capacity of MS.

3.3 Adsorption isotherm

The adsorption characteristics of the inhibitors can be summarized based on the nature of corrosion inhibition. The efficiency of a corrosion inhibitor mainly depends on its adsorption ability on the metal surface. So, it is necessary to know the mechanism of adsorption and the adsorption isotherm that can give valuable information on the interaction between the inhibitor and the metal surface. The surface protection of MS depends upon how the inhibitor molecule will be adsorbed on the metal surface, and also ionization and polarization of molecules [25]. The degree of surface coverage (θ) as function of concentration (C) of the inhibitor was studied graphically by fitting it to various adsorption isotherms to find the best adsorption isotherm. Langmuir adsorption isotherm was found to be the best description for all the studied inhibitors on MS in 0.5 M HCl medium. According to this isotherm, θ is related to the inhibitor concentration, C and adsorption equilibrium constant, K_{ads} through the following expression:

$$C/\theta = \frac{1}{K_{ads}} + C \tag{8}$$

Plots of C/θ versus C (fig. 4) yielded straight lines with the linear correlation coefficient (R^2) values close to unity, which suggests that the adsorption of INTMH, INMFA and INBHT in 0.5 M HCl medium on MS surface obeys the Langmuir adsorption isotherm. The slopes of the above plots are in the range of 0.952 to 1.056, suggesting that the adsorbed molecules form monolayer on the MS surface and there is no interaction among the adsorbed inhibitor molecules.

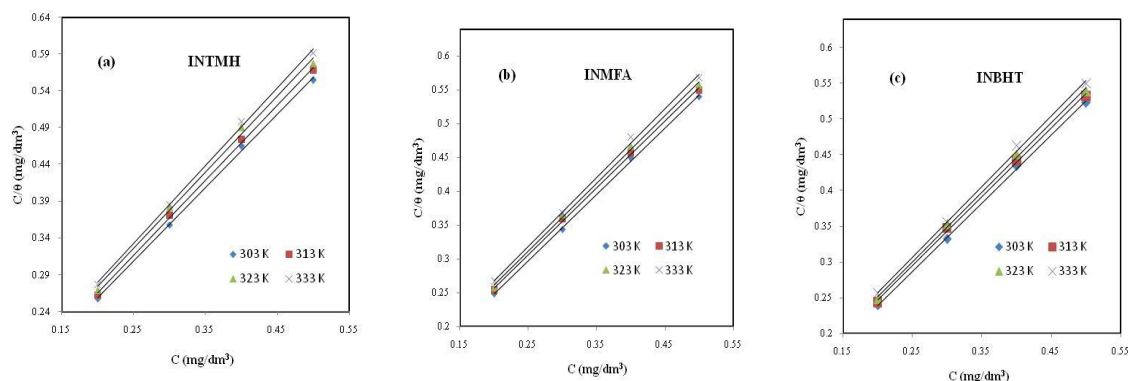


Figure (4): Langmuir’s adsorption isotherm plots for the adsorption of (a) INTMH (b) INMFA and (c) INBHT in 0.5 M HCl on MS surface at different temperature.

The Gibbs free energy of adsorption was calculated using the relation (9).

$$\Delta G_{ads}^{\circ} = -2.303RT \log 55.5 K_{ads} \tag{9}$$

where R is the universal gas constant, T is the absolute temperature, K_{ads} is the equilibrium constant for adsorption-desorption process and 55.5 is the molar concentration of water in solution (mol L^{-1}). The other adsorption thermodynamic parameters such as enthalpy of adsorption (ΔH_{ads}°) and entropy of adsorption (ΔS_{ads}°) are obtained from the slope and intercept of the plot of $\ln K_{ads}$ versus $1/T$ (fig. 5) using the equation (10).

$$\log K_{ads} = \frac{1}{2.303} \left(-\frac{\Delta H_{ads}^{\circ}}{RT} \right) + \left(\frac{\Delta S_{ads}^{\circ}}{R} \right) \tag{10}$$

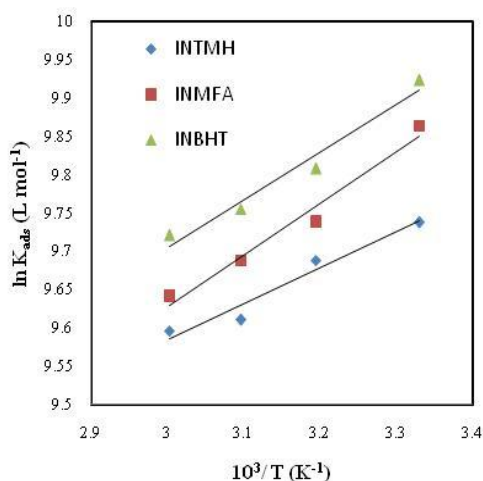


Figure (5): Plot of $\ln K_{ads}$ versus $1/T$ for INTMH, INMFA and INBHT.

The calculated values of K_{ads} , ΔH°_{ads} , ΔG°_{ads} and ΔS°_{ads} over the temperature range 30 – 60 °C are recorded in Table (3). Lagrenee et al., have reported that higher the K_{ads} value, the stronger and more stable adsorbed layer is formed which results in the higher inhibition efficiency [26].

Table (3): Thermodynamic parameters for adsorption of INTMH, INMFA and INBHT on MS in 0.5 M HCl at different temperatures

Inhibitor	T (°C)	R ²	K _{ads} (L mol ⁻¹)	-ΔG [°] _{ads} (kJ mol ⁻¹)	ΔH [°] _{ads} (kJ mol ⁻¹)	ΔS [°] _{ads} (J mol ⁻¹ K ⁻¹)
INTMH	30	0.998	16949.15	34.65	0.466	8.187
	40	0.998	16129.03	35.67		
	50	0.996	14925.37	36.60		
	60	0.998	14705.88	37.69		
INMFA	30	0.999	19230.76	34.97	0.676	7.598
	40	0.998	16949.15	35.79		
	50	0.998	16129.03	36.80		
	60	0.998	15384.61	37.81		
INBHT	30	0.999	20408.16	35.12	0.622	7.837
	40	0.999	18181.81	35.98		
	50	0.998	17241.37	36.98		
	60	0.998	16666.66	38.04		

The negative values of ΔG°_{ads} indicate the spontaneous adsorption of inhibitor on the surface of MS [27]. The values of ΔG°_{ads} are associated with water adsorption / desorption equilibrium which forms an important part in the overall free energy changes. In the present study, ΔG°_{ads} values for INTMH, INMFA and INBHT were found to be in the range -34.65 to -37.69, -34.97 to -37.81 and -35.12 to -38.04 kJ mol⁻¹, respectively in the temperature range of 30 – 60 °C, indicating that the adsorption is more physical than chemical [28-31].

3.4 FTIR spectral studies

FTIR spectra were recorded to understand the interaction of inhibitor molecules with the metal surface. figs. (6a), (7a) and (8a) show the FTIR spectra of pure INTMH, INMFA and INBHT. figs. (6b), (7b) and (8b) represent the FTIR spectra of the scratched samples obtained from the metal surfaces after corrosion experiments. Comparison between the FTIR spectra of pure inhibitors and inhibitor film removed mechanically from MS surface was performed. The azomethine group stretching frequencies for pure INTMH, INMFA and INBHT were found to be at 1662, 1628 and 1640 cm⁻¹, and carbonyl stretching frequencies were observed at 1761, 1750 and 1692 cm⁻¹, respectively. In the FTIR spectra of scratched samples, the stretching frequencies of the azomethine and carbonyl groups are found to be disappeared in all the cases. These observations confirm that the azomethine and carbonyl groups of INTMH, INMFA and INBHT are involved in the complex formation with the metal.

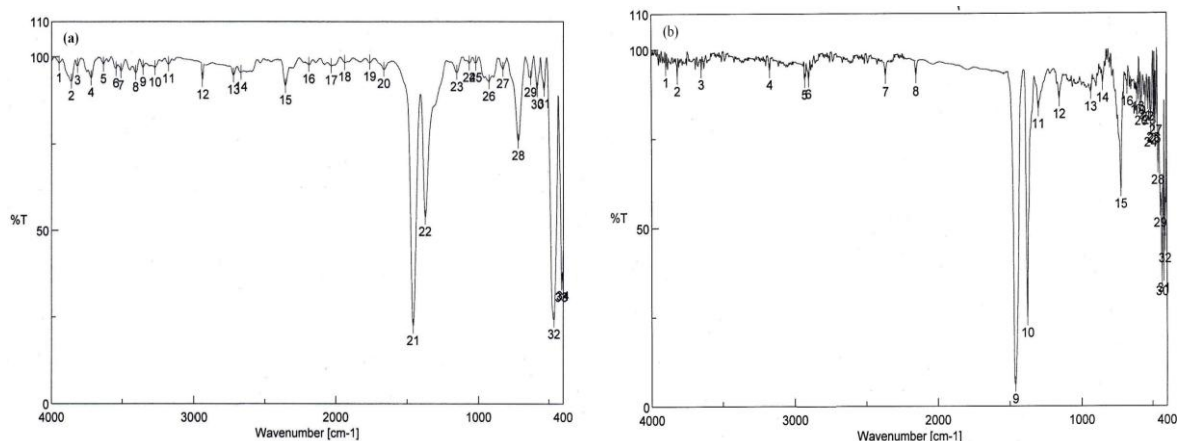


Figure (6): FTIR spectra of (a) INTMH and (b) scratched MS surface adsorbed INTMH film.

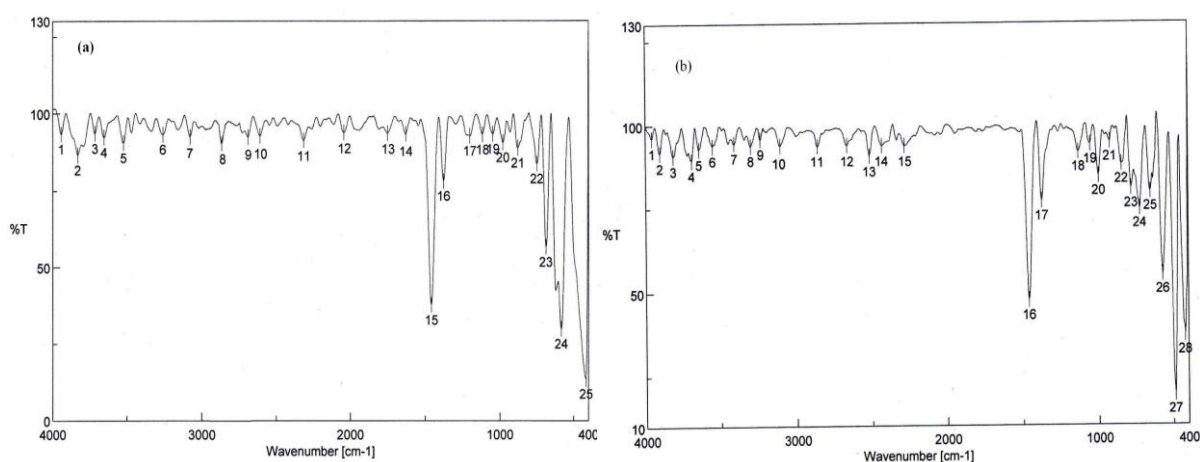


Figure (7): FTIR spectra of (a) INMFA and (b) scratched MS surface adsorbed INMFA film.

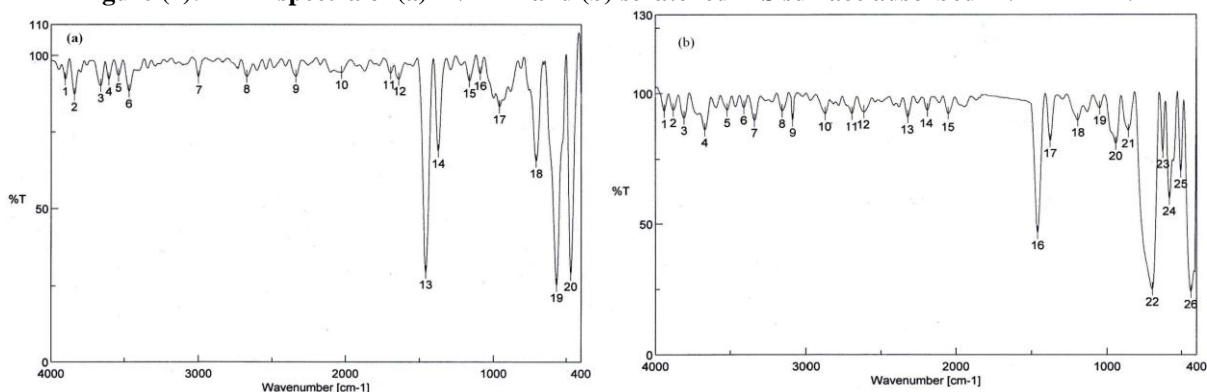


Figure (8): FTIR spectra of (a) INBHT and (b) scratched MS surface adsorbed INBHT film.

3.5 Potentiodynamic polarization studies

Inspection of fig. (9) reveals a typical polarization curves for MS in 0.5 M HCl in the absence and the presence of different concentrations of INTMH, INMFA and INBHT at 30 °C. The Tafel extrapolation plot showed that the addition of inhibitors hindered the acid attack on the mild steel electrode. In all the cases, addition of inhibitors reduces both anodic and cathodic current densities, indicating that these inhibitors exhibit cathodic and anodic inhibition effects, hence they are relatively mixed type of inhibitors [32, 33].

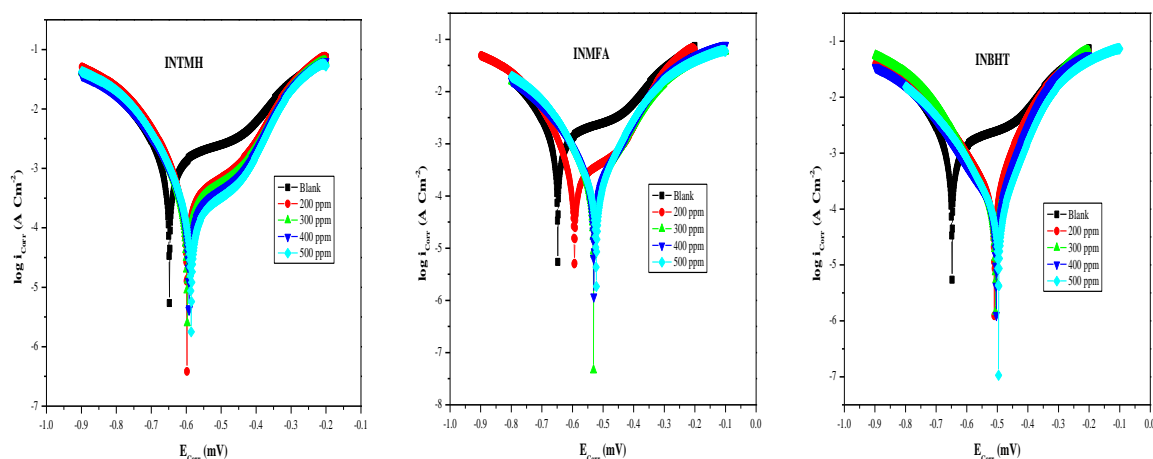


Figure (9): Polarization curves of MS in 0.5 M HCl in the presence of different concentrations of INTMH, INMFA and INBHT.

Lower the corrosion current density lesser will be the electron transfer in the redox process, therefore the rate of corrosion reaction becomes slower. Usually, a low current density and the presence of long anodization time represent a very good protection against corrosion due to the diminution of the porosity of the anodic films formed. Inspection of data in table (4) clearly shows that, as the concentration of the inhibitors increases there is a gradual decrease in the values of the corrosion potential and corrosion current. The values associated with electrochemical polarization parameters such as corrosion current density (i_{corr}), corrosion potential (E_{corr}), corrosion rate and η (%) determined from the polarization plots are given in Table (4).

Table (4): Polarization parameters and corresponding inhibition efficiency for the corrosion of the MS in 0.5 M HCl without and with various concentrations of INTMH, INMFA and INBHT at 30 °C

Inhibitor	C (ppm)	$-E_{corr}$ (mV)	i_{corr} ($\mu A cm^{-2}$)	η (%)
Blank	0	0.648	1661	-
INTMH	200	0.598	357.5	78.47
	300	0.597	303.8	81.70
	400	0.592	230.1	86.51
	500	0.586	162.4	90.22
INMFA	200	0.594	260.1	84.34
	300	0.531	187.1	88.73
	400	0.530	177.1	89.33
	500	0.522	121.2	92.70
INBHT	200	0.510	227.8	86.28
	300	0.506	120.6	92.73
	400	0.503	113.6	93.16
	500	0.496	79.52	95.21

It is evident that, η (%) increases with inhibitors concentration, and protection action of INTMH, INMFA and INBHT can be attributed to the electron density of the azomethine ($-C=N-$) group and this electron density varies with the substituents in the inhibitor molecules. The imine nitrogen can donate the lone pair of electrons to the metal surface more easily and hence reduce the corrosion rate. The η (%) was found to be in the order, INBHT>INMFA>INTMH, which can probably be explained on the basis of the additional functional groups and also the nature of the hetero atoms in the inhibitor molecules.

3.6 Electrochemical impedance spectroscopy (EIS)

The Nyquist plots for MS in 0.5 M HCl solution with and without different concentrations of INTMH, INMFA and INBHT was shown in fig. (10). The EIS diagram corresponds to reaction impedance which can be attributed to the charge transfer reaction of the MS corrosion process and also diffusion process across the corrosion layer.

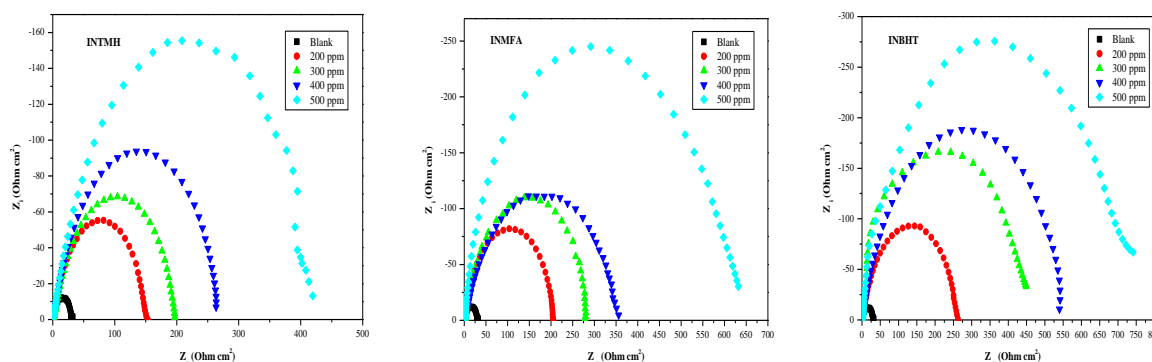


Figure (10): Nyquist plots for MS in 0.5 M HCl in the presence of different concentrations of INTMH, INMFA and INBHT.

Nyquist plots are regarded as one part of a semicircle mostly referred to as frequency dispersion which could be attributed to different physical phenomenon such as roughness, heterogeneities, impurities, grain boundaries and distribution of the surface active sites [34]. The electrochemical impedance parameters derived from the Nyquist plots and η (%) are listed in Table (5).

Table (5): Impedance parameters for the corrosion of MS in 0.5 M HCl in the absence and presence of different concentrations of INTMH, INMFA and INBHT at 30 °C

Inhibitor	C (ppm)	R_{ct} ($\Omega \text{ cm}^2$)	C_{dl} ($\mu\text{F cm}^{-2}$)	η (%)
Blank	0	27.99	315.7	-
INTMH	200	128.4	102.4	78.20
	300	153.3	76.84	81.74
	400	205.0	72.66	86.34
	500	326.5	72.23	91.42
INMFA	200	183.1	70.37	84.71
	300	239.7	56.88	86.34
	400	256.5	49.07	89.08
	500	542.9	45.16	94.84
INBHT	200	203.2	65.25	86.22
	300	391.9	53.3	92.85
	400	408.0	42.47	93.13
	500	610.0	41.33	95.41

From the plots it is clear that the impedance response of MS in uninhibited acid solution has significantly changed after the addition of inhibitors to the corrosive solution. This indicates that the impedance of the inhibited metal increases with increasing concentration of the inhibitors. The measured impedance data were based upon the equivalent circuit given in the fig. (11), consists of constant double layer capacitance (C_{dl}) in parallel with polarization resistance (R_p) which is in series with solution resistance (R_s).

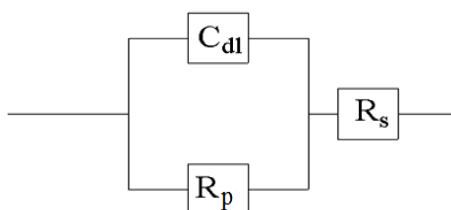


Figure (11): Equivalent circuit used to fit the impedance spectra.

The value of R_p is a measure of electron transfer across the surface, and inversely proportional to the corrosion rate. It was clear that, R_p values in the absence of the inhibitors are always lower than those in the presence of the inhibitors. The increase in the R_p values in the presence of different concentrations of INTMH, INMFA and INBHT indicate reduction in the MS corrosion rate with the formation of adsorbed protective film on the metal-solution interface [35, 36]. When the concentration was raised from 200 - 500 ppm, there was a gradual increase in the diameter of each semi-circle of the Nyquist plot. This reflecting the increase of R_p values

from 27.99 to 326.5, 542.9 and 610.0 $\Omega \text{ cm}^2$ for INTMH, INMFA and INBHT, respectively, suggesting that the formed inhibitive film was strengthened by addition of inhibitors.

The double layer capacitance (C_{dl}) values were decreased due to decrease in local dielectric constant and / an increase in the thickness of the electrical double layer, suggesting that the inhibitor molecules adsorbed at the metal-solution interface^[37, 38]. Decrease in the surface area^[39] and imperfections of the metal surface may also be the reason for decrease of C_{dl} values. Addition of inhibitors provided lower C_{dl} values because of the replacement of water molecules by inhibitor molecules at the electrode surface^[40]. It was clear that, as the immersion time increases the R_p values increases and C_{dl} values decreases which indicate the higher protection efficiency as a result of slow adsorption of inhibitor molecules on to the MS surface. However, when the immersion time is further enhanced, a sudden decrease in R_p values and increase in C_{dl} values were observed. This behaviour can be due to the instability of the passive film or desorption of the inhibitor molecules.

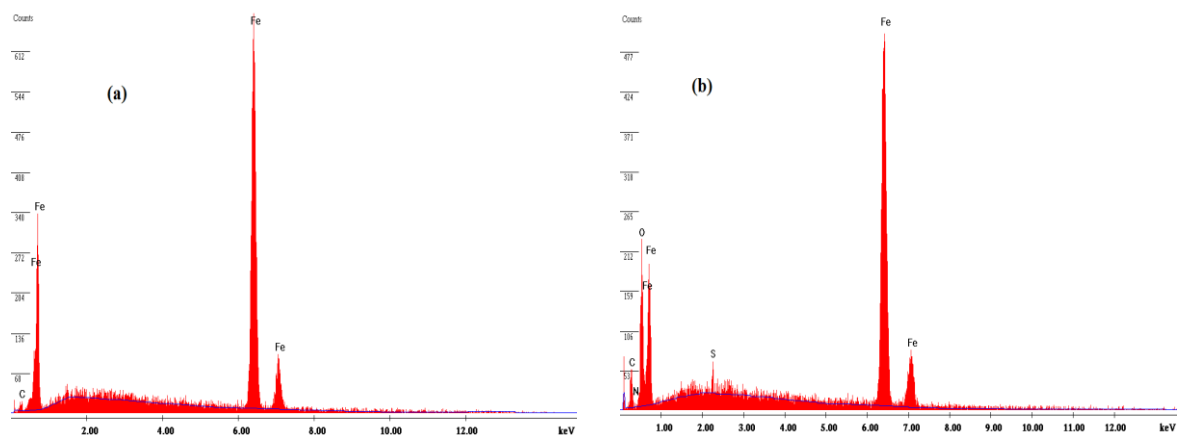
3.7 Mechanism of inhibition

The inhibition effect of isoniazide derivatives towards the corrosion of MS in 0.5 M HCl solution is attributed to the adsorption of these compounds at the metal-solution interface. The principal types of interaction between an organic inhibitor and metal surface are physisorption, chemisorption or both. The adsorption of inhibitor is influenced by the nature of the metal, chemical structure of inhibitors, type of aggressive electrolyte, temperature and the morphology of MS surface^[41, 42]. The values of inhibition efficiency depend essentially on the electron density at the active centre of the inhibitor molecule. Chemisorption of these inhibitors arises from the donor - acceptor interactions between the free electron pairs of hetero atoms and π -electrons of multiple bonds as well as phenyl group and vacant d orbitals of iron^[43, 44].

In the case of INTMH, the inhibition effect is due to the interaction of π -electrons of thiophene and pyridine rings as well as the presence of electron donor groups (S, N, O and C=N) through which it form bonds with the metal. In the similar way, the inhibition effect in INMFA is due to π -electrons of phenyl and pyridine rings, presence of S, N, O, C=N and CH_3 . In the case of INBHT it is due to π -electrons of phenyl and pyridine rings, presence of S, N, O and C=N, through which the inhibitors adsorb on the MS surface forming insoluble, stable and uniform thin film. The highest inhibition efficiency of INBHT is due to the presence of sulphur atom adjacent to the azomethine group which provides a high electron density. Indeed, Chetouani et al^[45] reported the importance of sulphur atom and drastic change of adsorption mechanism. INMFA comes after INBHT, this is due to the presence of electron donating $-\text{CH}_3$ group adjacent to nitrogen atom which is in turn attached to azomethine group. INTMH is the least effective among the studied inhibitors.

3.8 EDX analysis

EDX spectra were used to determine the elements present on MS surface before and after exposure to the inhibitor solution. The results are displayed in fig. (12a) – (12d). fig. 12a is the EDX spectrum of the polished MS sample and it is notable that the peak of oxygen is absent which confirm the absence of air formed oxide film. However, for inhibited solutions (fig. 12b) the additional lines characteristic for the existence of S, N and O (due to S, N and O atoms of INTMH) in the EDX spectrum are observed. In the similar way fig. (12c) showed additional lines characteristic for the existence of N and O (due to N and O atoms of INMFA), and fig. (12d) showed additional lines characteristic for the existence of S, N and O (due to S, N and O atoms of INBHT) in the EDX spectrum. These data showed that S, N and O atoms of inhibitors are involved in bonding with the MS surface. These results confirm the observations of FTIR and SEM studies.



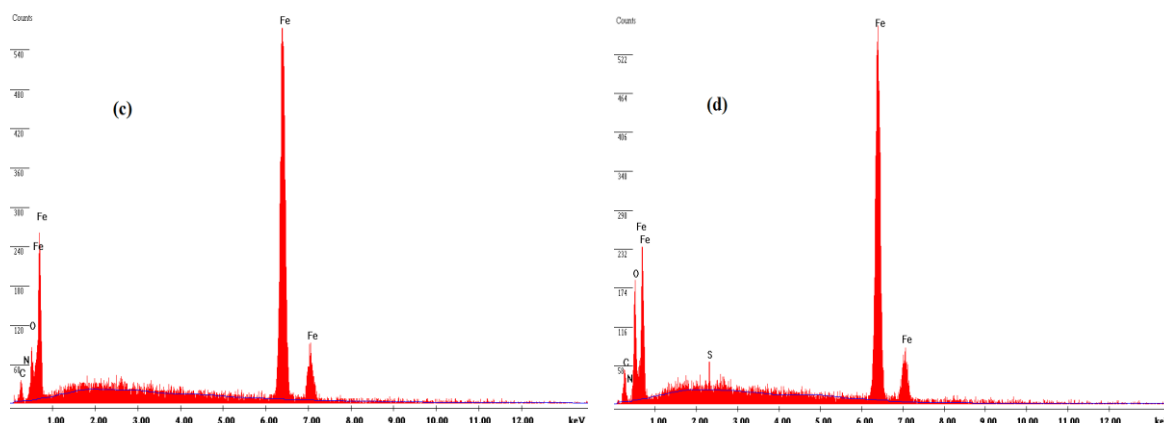


Figure (12): EDX images of (a) polished MS surface (b) MS in 500 ppm INTMH (c) MS in 500 ppm INMFA and (d) MS in 500 ppm INBHT.

3.9 SEM analysis

SEM images of the polished and corroded MS surface in the absence and the presence of inhibitors are displayed in figs. (13a-13e). fig. (13a) represents the SEM image of polished MS surface. fig. (13b) is the SEM image of MS surface in 0.5 M HCl without inhibitor, which clearly shows the pitting behaviour and cracks. However, SEM images of MS surface in the presence of inhibitors (figs. (13c), (13d) and (13e)) were observed to be homogeneous and less cracked than that of MS surface in 0.5 M HCl alone. The interpretation of these SEM observations reveals that the inhibitors form a thin protective layer on the MS surface, which prevents the attack of acid as well as the dissolution of MS by forming a surface adsorbed layer and thereby reducing the corrosion rate.

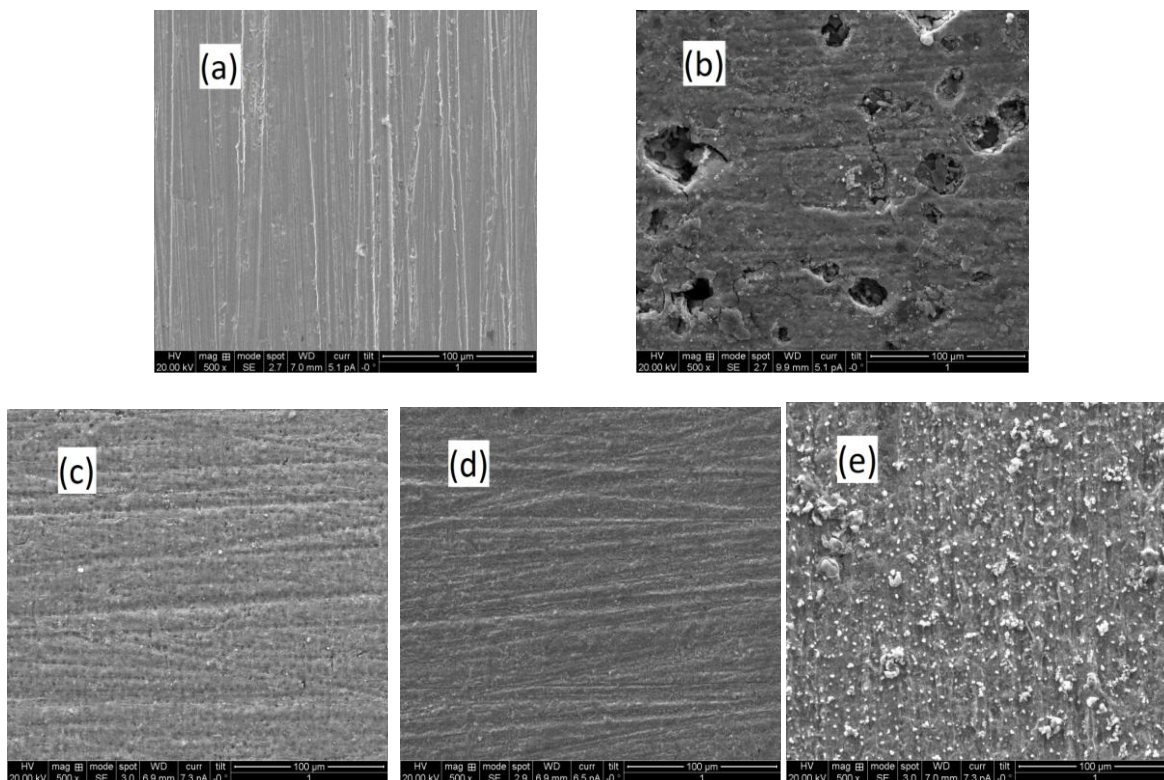


Figure (13): SEM images of (a) polished MS surface (b) MS in 0.5 M HCl (c) MS in 500 ppm INTMH (d) MS in 500 ppm INMFA and (e) MS in 500 ppm INBHT.

IV. Conclusion

1. Corrosion behaviour of MS was studied and compared in the absence and presence of different concentrations of inhibitors using electrochemical, non-electrochemical, FTIR, EDX and SEM techniques.
2. Electrochemical and non-electrochemical studies are in good agreement with each other, and the inhibition efficiency was found in the order: INBHT>INMFA>INTMH.
3. Langmuir adsorption isotherm was found to be the best description for all the studied inhibitors.
4. The difference in the inhibitory properties of the inhibitors is related to the difference in the structure, composition and also presence of functional groups containing hetero atoms in the inhibitor molecules.
5. SEM and EDX studies showed the existence of protective film of inhibitors on MS surface.

Acknowledgements

One of the authors (MPC) is grateful to University of Mysore, Mysore for awarding SRF to carry out the research work.

References

- [1]. A.M. Fekry, and R.R. Mohamed, *Electrochim. Acta*, 55, 1933, 2010.
- [2]. M. Abdulla, M. Al-Agez, and A.S. Fouda, *Int. J. Electrochem. Sci.*, 4, 336, 2000.
- [3]. Wang Hui-Long, Liu Rui-Bin, and Xin Jian, *Corros. Sci.*, 46, 2455, 2004.
- [4]. Emregul Kaan, Kurtaran Raif, and Atakol Orhan, *Corros. Sci.*, 45, 2803, 2003.
- [5]. M.A. Quraishi, and R. Sardar, *Mater. Chem. Phys.*, 78, 425, 2003.
- [6]. M. Sachin, S. Bilgic, and H. Yilmaz, *Appl. Surf. Sci.*, 195, 1, 2002.
- [7]. M.S. Abdallah, O. Al Karanea, and A.A. Abdel Fataha, *Chem. Eng. Comm.*, 197, 1446, 2010.
- [8]. M. Bouklah, A. Aouniti, B. Hammouti, M. Benkaddour, M. Lagrenee, and F. Bentiss, *Prog. Org. Coatings*, 51, 118, 2004.
- [9]. F. Bentiss, M. Traisnel, H. Vezin, H.F. Hildebrand, and M. Lagrenee, *Corros. Sci.*, 46, 2781, 2004.
- [10]. M. Karakus, M. Sahin, and S. Bilgic, *Mater. Chem. Phys.*, 92, 565, 2005.
- [11]. A. Afidah, E. Rahim, J. Rocca, M.J. Steinmetz, R.A. Kassim, and M. Sani Ibrahim, *Corros. Sci.*, 49, 402, 2007.
- [12]. W. Li, Q. He, C. Pei, and B. Hou, *Electrochim. Acta*, 52, 6386, 2007.
- [13]. M. Benabdellah, B. Hammouti, A. Warthan, S.S. Al-Deyab, C. Jama, M. Lagrenee, and F. Bentiss, *Int. J. Electrochem. Sci.*, 7, 3489, 2012.
- [14]. M.A. Migahed, A.M. Abdul-Raheim, A.M. Atta, and W. Brostow, *Mater. Chem. Phys.*, 121, 208, 2010.
- [15]. M.Z.A. Rafiquee, Nidhi Saxena, Sadar Khan, and M.A. Quraishi, *Ind. J. Chem. Tech.*, 14, 576, 2007.
- [16]. Eno E. Ebenso, Taner Arslan, Fatma Kandemirli, Ian Love, Cemil Ogretir, Murat Saracoglu, and Saviour A. Umoren, *Int. J. Quan. Chem.*, 110, 2614, 2010.
- [17]. R.T. Loto, C.A. Loto, and A.P.I. Popoola, *J. Mater. Environ. Sci.*, 3, 885, 2012.
- [18]. S. Acharya, and S.N. Upadhyay, *Trans. Indian. Inst. Met.*, 57, 297, 2004.
- [19]. M. Abdallah, E.A. Heal, and A.S. Fouda, *Corros. Sci.*, 48, 1639, 2006.
- [20]. M.A. Quraishi, and Danish Jamal, *JAOCS*, 77, 1107, 2000.
- [21]. M.A. Quraishi, and Hariom K. Sharma, *Mater. Chem. Phys.*, 78, 18, 2002.
- [22]. Ambrish Singh, Ashish Kumar Singh, and M.A. Quraishi, *The open Electrochem. J.*, 2, 43, 2010.
- [23]. M.A. Quraishi, V. Bhardwaj, and J. Rawat, *JAOCS*, 79, 603, 2002.
- [24]. T. Poornima, J. Nayak, and A.N. Shetty, *Chem. Sci. J.*, 69, 1, 2012.
- [25]. S.A.M. Refaey, F. Taha, and A.M. Abd El-Malak, *Int. J. Electrochem. Sci.*, 1, 80, 2006.
- [26]. M. Lagrenee, B. Mernari, M. Bouanis, M. Traisnel, and F. Bentiss, *Corros. Sci.*, 44, 573, 2002.
- [27]. S.A. Umoren, and E.E. Ebenso, *Mater. Chem. Phys.*, 106, 387, 2007.
- [28]. M. Bouklah, B. Hammouti, M. Lagrenee, and F. Bentiss, *Corros. Sci.*, 48, 2470, 2006.
- [29]. F.M. Bayoumi, and W.A. Ghanem, *Mater. Letts.*, 59, 3806, 2005.
- [30]. A. Yurt, A. Balaban, S. Ustun Kandemir, G. Bereket, and B. Erk, *Mater. Chem. Phys.*, 85, 420, 2004.
- [31]. X. Li, S. Deng, H. Fu, and T. Li, *Electrochim. Acta*, 54, 4089, 2009.
- [32]. M. Lebrini, F. Bentiss, H. Vezin, and M. Lagrenee, *Appl. Surf. Sci.*, 252, 950, 2005.
- [33]. Ahmed Y. Musa, Abdul Amir H. Kadhum, Abu Bakar Mohamad, Mohd Sobri Takriff, Abdul Razak Daud, and Siti Kartom Kamarudin, *Corros. Sci.*, 52, 526, 2010.
- [34]. K. Juttner, *Electrochim. Acta*, 35, 1501, 1990.
- [35]. F. Bentiss, M. Lebrini, M. Langrenee, M. Traisnel, A. Elfarouk, and H. Vezin, *Electrochim. Acta*, 52, 6865, 2007.
- [36]. F. El-Taib Heakal, A.A. Ghoneim, and A.M. Fekry, *J. Appl. Electrochem.*, 37, 405, 2007.
- [37]. M. Lebrini, F. Bentiss, H. Vezin, and M. Lagrenee, *Corros. Sci.*, 48, 1279, 2006.
- [38]. S.K. Shukla, and M.A. Quraishi, *Corros. Sci.*, 52, 314, 2010.
- [39]. F. Bentiss, M. Traisnel, and M. Lagrenee, *Corros. Sci.*, 42, 127, 2000.
- [40]. K. Parameswari, S. Chaitra, C. Nusrath Unnisa, and A. Selvaraj, *J. Appl. Sci. Res.*, 6, 1100, 2010.
- [41]. S. Aloui, I. Forsal, M. Sfaira, M. Ebn Touhami, M. Taleb, M. Filali Baba, and M. Daoudi, *Portugaliae Electrochim. Acta*, 27, 599, 2009.
- [42]. I. Zaaferany, *Portugaliae Electrochim. Acta*, 27, 631, 2009.
- [43]. M. Behpour, S.M. Ghoreishi, M. Salavati-Niasari, and B. Ebrahimi, *Mater. Chem. Phys.*, 107, 153, 2008.
- [44]. I. Ahamad, and M.A. Quraishi, *Corros. Sci.*, 51, 2006, 2009.
- [45]. A. Chetouani, A. Aouniti, B. Hammouti, N. Benchat, T. Benhadda, and S. Kertit, *Corros. Sci.*, 45, 1675, 2003.